AUTO OSCILLATIONS IN AXISYMMETRIC PULSED JET GENERATOR, HIGH-FREQUENCY MODE ASSOCIATED WITH CAVERN BOUNDARY INSTABILITY

© 2025 S. A. Ocheretyanyi*, V. V. Prokofiev, E. V. Topeytsev, E. V. Filatov**

Lomonosov Moscow State University, Research Institute of Mechanics, Moscow, Russia

**e-mail: ocheret@imec.msu.ru*

***e-mail: vlad.prokof@yandex.ru*

Received March 31, 2025

Revised April 25, 2025

Accepted april 25, 2025

Abstract. Research of liquid jet flows in the presence of a ventilated cavern with a negative cavitation number, conducted at the Institute of Mechanics of Moscow State University, has shown that under certain conditions in the hydraulic system cavitation auto-oscillations with high intensity of pressure pulsations occur. The paper presents the results of research of an axisymmetric model of a pulse jet generator with liquid jet flow through the central orifice in the diaphragm and with peripheral gas blow-up behind the diaphragm. The two-phase medium flowing outward was realized through a tapered conical nozzle. Research on the influence of the generator parameters as well as the distance to the screen wall on its efficiency was carried out. A narrow region of relatively small blow-ups was found, in which pressure fluctuations with high frequency are registered, and the amplitude of pressure shock pulses on the screen noticeably exceeds the amplitude of pulses in low-frequency modes of generation. This mode may be a consequence of the development of two-phase structures at the unstable boundary of the jet during its interaction with the walls of the tapered nozzle. Proof of the possibility of the existence of such a flow regime was the solution of a plane problem on the interaction of a finite jet with an inclined plate at different pressures on the jet surfaces. The problem is solved exactly by TFCP methods using quasi-binary-periodic theta functions.

Keywords: *jet flow, cavern, negative cavitation number, cavitation autoconvulsions, pulsation technologies*

DOI: 10.31857/S10247084250302e3

INTRODUCTION

Research of jet fluid flows in the presence of a ventilated cavern with a negative cavitation number, conducted at the Institute of Mechanics of Moscow State University [1-3] showed that under certain conditions in the hydraulic system there are cavitation auto-oscillations with high intensity of pressure pulsations both in the cavern and in the region upstream. The possibility in principle of using the auto-oscillation mode to create periodic pulse jets when flowing from a tapered nozzle into the atmosphere was shown. The most obviously application of the pulse jet generator can be found in the technologies of water-jet mining [4]. To obtain jets with very high parameters, pulse water cannons (the liquid receives impulse due to the impact of a piston accelerated by powder gases) and hydrocannons (the liquid in the shaft is accelerated together with the piston) are usually used. The scheme without piston pulse water cannon has the closest relation to the topic considered in the article: the liquid mass is accelerated directly by gas. Calculations and experiment [4, 5] have shown that the velocity of such jets can reach 1600 m/s with a sufficiently large range when flowing both into the air and into the space flooded with water.

In plants using pulsating jets, there is a noticeable increase in productivity and, at the same time, a decrease in the specific energy intensity of material destruction and a decrease in water consumption, which ensures the permissible moisture content of the extracted mineral. In [6] a review of devices capable of providing pulsation mode of operation of jet plants is given. As a rule, mechanical devices are used in such installations to organize pulsating modes of operation. However, there are known ways to create pulse jets without using mechanical devices - first of all, these are pulse jet generators that use cavitation auto-oscillations at occurrence of natural (steam) cavitation in a Venturi tube [7]. The operation of such generators assumes a significant pressure drop at the inlet and outlet of the Venturi tube and starts at rather high head pressures sufficient for the development of vapor cavitation in the channel of the Venturi tube. For the generator scheme studied here, the presence of a ventilated cavern behind the cavitator is fundamental, the character of the flow changes: intensive auto-oscillations occur at small pressure drops on the cavitator, the energy of impulse jets includes not only the liquid head, but also the work of compressed gas. As a result, developed cavitation autocolevations begin already at small (less than 0.01 MPa) head pressures. Note that in generators using natural cavitation in a Venturi tube, the presence of an outlet tapered nozzle is not fundamental (the generator works effectively without such a nozzle [8]), while in a scheme with a ventilated cavern, the presence of an outlet nozzle (or other resistance) is fundamental.

The question of generating periodic pulsed jets using cavitation auto-oscillations was previously studied in a planar formulation [9]. However, for practical purposes, the axisymmetric formulation of the experimental problem is closer. Further research was carried out on an

axisymmetric model of the unit, and, at the first stage, a technologically simpler configuration with the liquid jet flowing through the central hole in the diaphragm and with peripheral gas blowing was produced (in the flat formulation, the flow with a central ventilated cavern was modeled). Experiments, showed that low-frequency auto oscillations also occur in this configuration, but at slightly higher coefficients of gas underblow than in the flat model with a central cavern [3], the intensity of shock pulses was somewhat lower than in the flat setup. Research on the influence of nozzle parameters on the generator efficiency was carried out, and the dependence of the intensity of shock pulses on the distance to the wall-screen was investigated.

Experiments have shown that there is a narrow region of relatively small blow-ups in which pressure fluctuations with a frequency much higher than the frequency of fluctuations developing at large blow-ups are registered. The amplitude of these high-frequency pressure oscillations in the cavern is very small, however, it is in this narrow region that the mode with the formation of pressure pulses on the target screen, the amplitude of which significantly exceeds the amplitude of low-frequency pulses is realized. It is clear that for appendixes such a flow regime is very favorable. Previously, the regime with an unstable Rayleigh-Taylor cavern was observed in the flow with the central position of the cavern, while here it takes place at the interaction of the central jet with the walls of the tapered nozzle at the generator outlet. Proof of the existence of such a regime was the solution of the plane problem of the interaction of a finite jet bounded from below by a plane wall (plane of symmetry) with an inclined plate at different pressures on the surfaces of the jets above and below the inclined plate. Similar to the plate gliding problem, a flow scheme with jet separation was adopted. The problem has been solved exactly by TFCP methods using quasi-double-joint-periodic theta functions. The analysis of the solution shows that the Rayleigh-Taylor (R-T) instability of the jet boundary takes place near the limiting flow when the thickness of the return jet turns to zero (the jet touches the inclined plate at some point above the disruptive edge of the plate). The obtained solution, in particular, explains the narrowness of the range of values of the dimensionless pressure coefficient in the cavern C_d, at which high-frequency auto oscillations take place. Estimates have shown that, in the presence of an unstable boundary, the development of wave structures may well lead to the destruction of the jet into fragments. For the plane problem, the dependences of the limiting flow parameters on the plate inclination angle and the width of the gap between the plate edge and the plane wall are obtained.

1. RESEARCH OF AUTO-OSCILLATORY MODES OF FLOW IN AXISYMMETRIC GENERATOR OF PULSE JETS

1.1 Description of the experiment

Previously, on a flat experimental setup [9, 10], a flow with the formation of a ventilated cavern behind a cavitator plate (or wedge) in the central part of a two-phase flow was modeled. Here, in the axisymmetric case, the flow with a liquid jet in the central part of the flow is organized. Fig. 1 shows a scheme of axisymmetric two-phase flow in the stationary regime. From the pressure pipe *1* the liquid through the hole in the washer (cavitator) *2* enters the chamber *3*, into which the air is blown. From the chamber *3* there is a smooth transition to the cylindrical part of the outlet nozzle *4*, which ends with a conical constriction *5*. The jet flows into the tank (not shown on the scheme) where a screen (disk) *6* is installed, in the center point of which there is a hole for pressure measurement. In the course of the experiment the oscillograms of pressure in the supply line (in front of the washer-cavitator *2*) p_0, in the cavern *3* behind the cavitator p_k, in the central point of the screen *6* - p_m are recorded (pressures are measured relative to atmospheric p_a). Liquid (water) was supplied to the unit through a ~1.5 m long steel pipeline (not shown in the scheme), from an air-cushioned stilling tank with a total volume of 50 liters. The diameter of the washer at the generator inlet $D = 10$ mm, the inner diameter of the cylindrical part of the nozzle *4* also 10 mm. The distance from the nozzle cutoff to the screen *6* could be varied. In some experiments, the inlet washer *2* was replaced by a conical confuser. The element base and instruments for measuring experiments are given in [9].

1.2 Influence of outlet section diameter

Fig. 2-5 shows the influence of the nozzle outlet cross-section diameter on the character of auto oscillations for the head pressure P_0 – 0.15 MPa. Parameters of the generator channel: total length 57 mm (from the inlet washer to the nozzle shear), end conical nozzle with a transition from the diameter of the cylindrical part of the nozzle 10 mm to the outlet diameter d, distance to the target disk 25 mm. The following dimensionless parameters were determined in the experiments: cavern pressure coefficient $C_d = P_k/P_0$, Struhal number, $Sh = fD/V_\infty$, blow-up coefficient $C_q = Q_g/Q_l$, where Q_g is the volumetric flow rate of gas reduced to pressure P_k, Q_l is the liquid flow rate. The magnitude of pressure fluctuations in the forechamber A_0 and in the cavern A_k, and the intensity of shock pulses on the screen A_m, are related to the head pressure p_0. Large shafts P_0 and P_k denote time-averaged overpressures in the forechamber and in the cavern, $V_\infty = \sqrt{2P_0/\rho}$, f is the pulsation frequency, the oscillation sweep was also determined as the average value of the difference between maxima and minima at intervals equal to the oscillation period $1/f$. The diameter of the jet flowing out of the washer hole is 7.7 - 8.4 mm (depending on the Reynolds number). An important factor here is the ratio of the nozzle outlet diameter to the jet diameter. At an outlet diameter of 8 mm, the jet at steady-state flow interacts weakly with the nozzle walls and at small blow-ups there is actually a direct flow from the hole in the washer into the atmosphere (low values of C_d, no auto oscillations), however, at significant blow-ups (C_q >15) and in this case low-

frequency auto oscillations begin to develop and the C_d coefficient increases (Fig. 2, 4). It can be seen that in the regime of developed low-frequency oscillations the pressure coefficients in the cavern for exit diameters of 6 and 7 mm practically coincide, for the diameter of 5 mm the pressure coefficient increases.

Fig. 3 shows the dependences of the Struhal number on the blow-up coefficient C_q for the outlet nozzle diameters d = 8, 7, 6, 5 mm. The vertical scale was chosen so that the low-frequency mode of the auto-oscillations could be clearly seen (the second part of the paper is devoted to high frequencies at small blow-ups). It can be seen that at d = *8* mm the auto-oscillation mode occurs at $C_q > 16$. The oscillation frequency decreases with decreasing nozzle diameter, and for d = 6 and 7 mm, the results for Sh and for C_d are almost the same. The change in the frequency of auto-oscillations at other diameters of the outlet section can be related to the change in the pressure coefficient C_d, since it was previously shown [11, 12] that the velocity of wave propagation along the jet coincides with the velocity of the stationary jet.

Fig. 4 shows the dependence of the intensity of pressure pulsations in the cavern at P_0 = 0.15 MPa for the same four diameters of the nozzle outlet section. At d = 8 mm autocolevations begin to develop only at $C_q > 15$, in the range of C_q from 10 to 20 (where, by analogy with the flat problem, the mode of oscillations without gas ejection into the region in front of the cavitator should be preserved) the intensity is greater the smaller the diameter of the outlet section, however, in the range of 5-7 mm the intensity of autocolevations (A_k/P_0) weakly depends on the outlet diameter. Fig. 5 shows the dependence of the average screen impact intensity A_m/P_0 on C_q. It can be seen that at d = 8 mm the impact is negligible, with the highest impact at d = 7 mm. In the low-frequency generation mode, the pulse amplitude increases with increasing underblow and reaches a maximum when switching to the mode with gas ejection in the region in front of the cavitator.

1.3 Dependence of intensity of the jet impact on the screen on the distance to the screen

Figs. 6-9 presents the results of measurements of the parameters of the auto-oscillatory mode of flow in the channel at the total length of the axisymmetric channel 57 mm, the length of the cylindrical part of the nozzle 11 mm, the end conical nozzle with a transition from the diameter of 10 mm (cylindrical part of the nozzle) to the exit diameter of 6 mm at the head pressure P_0 = 0.15 MPa, at distances to the target disk L_m varying from 25 to 250 mm (4.17 -41.7 caliber of the nozzle exit cross-section). From the presented in Figs. 6-8 it can be seen that in the selected range of distances to the target, it does not affect the flow regime in the channel. The closeness of the curves indicates good repeatability of the experimental regimes. Depending on the value of the blow-up coefficient C_q the flow in the generator goes through several stages. In the region C_q<10 , with the increase of underblow, C_d grows, the development of the cavern behind the cavitator occurs, and there are no low-frequency pressure fluctuations in the cavern. As the cavern closure

region approaches the nozzle outlet cross-section, a high-frequency mode of autoconvulsions may occur, the nature of which differs from the low-frequency mode (this will be discussed below). At C_q >10 a low-frequency auto-oscillation mode develops. It can be seen that here the pressure coefficient C_d changes very slowly with increasing blow-up (see Fig. 6), the frequency is also almost constant (see Fig. 7). This can be explained by the fact that the speed of the waves on the surface of the cavern is equal to the speed of stationary fluid flow and is determined by the value C_d, and the time of existence of these shafts by the length of the channel from the diaphragm-cavitator to the nozzle outlet section is a constant value in this series of experiments. At this stage, the intensity of pressure fluctuations in the cavern increases, as well as the intensity of the unsteady jet impact on the target. In the region $C_q > 20$, the frequency of auto oscillations begins to fall, C_d increases, and the analysis of oscillograms shows that here the mode with ejection of portions of the blown gas into the region in front of the cavitator develops. From the data of Fig. 9, it follows that somewhere in the beginning of this region is the maximum impact of liquid portions on the target. The data of Fig. 9 show that the maximum intensity of pressure pulses corresponds to the initial stage of transition to the mode with gas ejection into the space in front of the cavitator. At small distances (25 mm is 4.17 caliber of the nozzle outlet section), the amplitude of pressure pulses on the target exceeds the liquid head pressure P_0 by a maximum of 3.5 times. It also noticeably exceeds the intensity of pressure pulsations in the cavern (see Fig. 8). As the distance to the target increases, the intensity of pressure pulses on the screen decreases. Approximations of the dependence of this intensity for some values of C_q (in the region of growth of the intensity of autocolevations) show that the intensity of the impact on the obstacle decreases approximately in proportion to the square root of the distance to it.

2. HIGH-FREQUENCY AUTO OSCILLATIONS AS A CONSEQUENCE OF INSTABILITY OF THE CAVERN BOUNDARY IN THE RAYLEIGH-TAYLOR SENSE

2.1 Example of high-frequency auto oscillations occurrence

Once again, let us consider the process of development of cavitation auto-oscillations for axisymmetric flow in the generator with the diameter of the inlet washer orifice 10 mm, the cylindrical part of the nozzle extended by 26 mm, the diameter of the outlet of the conical nozzle 6 mm, with the total length of the generator (washer, inlet chamber, cylindrical part, conical nozzle) 82 mm. Fig. 10a,b show the dependences of Sh and A_m/P_0 on C_q for two values of water head pressure. It follows from the data of Fig. 10a that there is a narrow region of relatively small blow-ups ($C_q < 4$), in which pressure oscillations with a frequency much higher than the frequency of oscillations developing at large blow-ups are registered. The amplitude of pressure fluctuations in the cavern at these modes is very small, however, the data of Fig. 10b show that it is in this

narrow region that the mode with the formation of pressure pulses on the screen, the amplitude of which significantly exceeds the amplitude of pulses in the low-frequency mode, is realized. It is clear that for appendixes such a flow mode is very favorable. Fig. 11a shows an oscillogram of pressure pulsations for the flow in a long generator (82 mm) with a relatively small gas underblow when the high-frequency mode takes place. The pressure in the cavern p_k (and in the water supply line p_0) is almost constant, however, the amplitude spectrum (Fig. 11b) clearly shows a dominant frequency coinciding with the frequency of shock pressure pulsations on the screen (Fig. 11c). In the region of interaction of the jet with the target disk, intense periodic pulses of shock character are observed (Fig. 11a). The oscillation spectra show that these pulses are strictly periodic (Fig. 11c), and their frequency coincides with the frequency of acoustic oscillations in the cavern, which allows us to make an assumption about the occurrence of an auto-oscillatory flow regime in the region of the cavern closure near the nozzle outlet section, with the cavern itself serving as a feedback element.

For a generator with a central cavern (this case was studied earlier in the flat setting), a high-frequency autoconvulsive regime was also observed, in which the main part of the cavern remained stationary, and mixing of liquid with gas was observed only in the cavern tail. It was believed that this mixing could be related to the Rayleigh-Taylor instability of the cavern boundary [15]. Below, in the flat formulation, it will be shown that a similar situation can occur in the case of a generator with a central location of the liquid jet.

2.2 Formulation of the plane problem

Generally speaking, the length of a stationary cavern will increase with increasing gas supply, similar to the problem of a cavern behind an obstacle in a channel [14]; in this problem, there is a limit number of cavitation at approaching which the length of the cavern tends to infinity. Since in our case the distance from the cavitator (a washer or wedge) to the outlet nozzle is sufficiently large, we will consider the regime of a developed cavern occupying the entire space from the cavitator at the inlet to the tapered nozzle at the outlet (as shown in Fig. 1). Then the problem can be divided into two: the first one is the jet flow from the channel with a tapered nozzle at the outlet (the area of the supply channel, cavitator and cavern behind it - 1, 2 and 3 in Fig. 1). In this case, the ratio of the expiring jet width h to the nozzle orifice width D is a function of the ratio of the orifice width to the supply channel width L and the nozzle angle $\pi\nu$ [14] . At $\nu = 1/2$, the nozzle is analogous to an axisymmetric washer. For the axisymmetric generator model parameters $D/L = 0.2$ and at $\nu = 1/2$, the ratio $h/D = 0.616$ (see [14]). When analyzing the second problem - the flow from the outlet nozzle 5 (see Fig. 1) - we will use the jet width h as the characteristic length.

The second problem - the interaction of a jet of width h with an inclined plate (constriction) with an inclination angleα - will be considered using a scheme with jet separation, which takes place when a jet of thickness *h* interacts with an inclined plate. One jet of thicknessΔ expires into space with constant pressure along a horizontally straight line (or symmetry axis), while the other jet (return jet of thicknessδ) flows along the inclined plate. Let us assume that the wall of the internal channel of the generator is far enough from the boundary of the jet *h* and we will neglect the influence of this wall (that is, we will consider the inclined wall to be infinite).

2.3 Problem on interaction of a finite jet with an inclined plate at different pressures on jet surfaces

Fig. 12a shows a stationary flow along the horizontal bottom of a layer of liquid (jet) with width at infinity (at point *E*) *h* interacting with a semi-infinite plate AC inclined with respect to the bottom (inclination angle$\alpha = \pi\mu$, when modeling a tapered nozzle $\mu > \pi/2$). When interacting with the inclined plate, the flow separates - part of it flows out into the space behind the plate (the velocity at the boundary of this jet is assumed to be 1). The boundary of the jet starts from the edge of the plate A and flows along the *x-axis* to infinity (point *D*), the other part flows along the inclined plate to infinity (point *C*). The point of flow separation B is the braking point on plate *AC*. Unlike the classical hydroplaning problem [14], here the pressures in front of and behind the plate are different.

The flow in the plane of the complex potential (Fig. 12b) is a flow in a strip in the presence of a cut that starts at the point of flow separation *B*. Note that the flow is bounded by straight lines $\psi = const$, at the boundaries of the region the imaginary part of the function w is constant. In [15] it is shown that a flow with boundaries made of rectilinear walls separated by two free surfaces with different values of velocity on them can be mapped onto a characteristic rectangle by means of an elliptic integral, and by a suitable choice of the parameter of the elliptic integral it can be made so that the four points of flow separation pass to the vertices of the characteristic rectangle. It is shown in the same [15] that the complex velocity is a quasi-bi-directional function.

We will construct the solution with the help of quasi-binary-periodic theta functions, using a procedure close to the one described in [14] (expressions for these functions, as well as some useful formulas, are given in the same monograph). Note that the first function ($\vartheta_1(u) = 2\sum_{n=1}^{\infty}(-1)^{n-1} q^{(2n-1)^2/4} \sin(2n-1)u \quad q = e^{\pi i \tau}, |q| < 1$) has a simple zero at the point $u=0$, and the

others are obtained from the first one by adding a real or complex half-period to the argument. As a parametric plane u (Fig. 12c) we choose a rectangle with sides equal to the half-periods of functions $\pi/2$ and $\pi\tau/2$, where $\pi\tau$ is the complex period of functions. Let us assume that point D of the physical plane passes to point u=0, point A to point $u = \pi/2$, point E to point $u = \pi\tau/2$. The fourth point - point C - passes to point $u = \pi/2 + \pi\tau/2$, where the complex parameter τ should be additionally determined from the problem conditions. So, the free boundaries go to the lower and upper sides of the rectangle, the solid rectilinear boundaries to the left and right sides. We will search for the solution by the method of special points [14]. The study of the velocity hodograph shows that the function dw/dz has one simple zero at the braking (and branching) point B ($u = \pi/2 + ia$), and due to the inversion with respect to the real axis in the analytic continuation, has a simple pole at $u = \pi/2 - ia$. In this case [14], the complex velocity can be represented as

$$\frac{dw}{dz} = Ae^{Bu}\frac{\vartheta_1(u - \pi/2 - ia)}{\vartheta_1(u - \pi/2 + ia)} = Ae^{Bu}\frac{\vartheta_2(u - ia)}{\vartheta_2(u + ia)}$$

where A and B are real constants that are determined from the conditions for the velocity at points $u=0, \left.\frac{dw}{dz}\right|_{u=0} = A = 1$ and A ( ), $u = \pi/2 \left.\frac{dw}{dz}\right|_{u=\pi/2} = e^{B\pi/2}\frac{\vartheta_2(\pi/2 - ia)}{\vartheta_2(\pi/2 + ia)} = e^{i(\pi-\beta)}$

As a result, for the complex velocity the following expression is obtained

$$\frac{dw}{dz} = e^{-2i\frac{\beta}{\pi}u}\frac{\vartheta_2(u - ia)}{\vartheta_2(u + ia)}$$

Using this expression and the condition for the velocity at the point $u = \pi\tau/2$

$$\left.\frac{dw}{dz}\right|_{u=\pi\tau/2} = e^{-i\beta\tau}\frac{\vartheta_2(\pi\tau/2 - ia)}{\vartheta_2(\pi\tau/2 + ia)} = e^{-i\beta\tau}e^{-2a} = v_0$$

for the complex period τ we obtain

$$\tau = i\,\frac{2a + \ln v_0}{\beta} \qquad (1)$$

Below we will consider the case when $v_0 < 1$ (the pressure in the cavern is elevated), that is, the logarithm in formula (1) is negative. Since the coefficient at i must be positive (a condition for convergence of series by which theta functions are represented [14]), it is required that $2a > |\ln v_0|$. But the choice of the constant a is bounded from above by $2a \le \pi|\tau|$. In the limiting case $2a = \pi|\tau|$ points C and B coincide (it will be shown below that the return jet vanishes in this case), and from relation (1) we obtain the limiting values of the parameters, which are determined only by the parameters of the problem v_0 and :β

$$|\tau| = \frac{\ln(1/v_0)}{\pi - \beta} \ (\text{or} 2a = \frac{\pi\ln(1/v_0)}{\pi - \beta}) \qquad (2)$$

When solving the problem, it is possible to set the nozzle width and find the corresponding parameter a (or $|\tau|$), but it is easier to do the opposite - to set a and get the nozzle width. The parameter a cannot be less than the value (2) , if the parameter a increases, the return jet will appear and the nozzle width will decrease. It should be added that the condition for the velocity

at the point $u = \pi/2 + \pi\tau/2$, when substituting into it the expression for the complex velocity taking into account formula (1), is fulfilled identically and does not give any additional relations.

The derivative of the potential on the parameter dw/du can be constructed by special points. The details of such a construction are available in the monograph [14], let us only mention the special points of the function dw/du . Since the function w has logarithmic singularities in the source (point E: $u = \pi\tau/2$) and in the sinks (points C and D: $u = \pi/2 + \pi\tau/2$, $u = 0$, , respectively), the derivative dw/du will have simple poles at these points. There are two special points with violation of conformality of the mapping - these are the branching point of the flow B ($u = ia$) and the corner point A ($u = \pi/2$) in them the function dw/du has zeros. Since we have to describe the special points of the function in the whole period [π, $\pi\tau$], we will add a zero in the point symmetric about the axis ($u = -ia$). Taking into account the special points, we can make the following combination of theta functions:

$$\frac{dw}{du} = N_1 \frac{\vartheta_2(u - ia)\vartheta_2(u + ia)\vartheta_2(u)}{\vartheta_1(u)\vartheta_3(u)\vartheta_4(u)}$$

This function is analytic and has simple poles and zeros corresponding to our flow in the entire rectangle [π, $\pi\tau$], and by virtue of the periodicity of theta functions describes singularities in the entire space u . Here N_1 is a real constant.

The constant N_1 , as well as the thickness of jets δ и Δ , let us determine using a formula that relates the intensities of sources (jets) at points E, C and D to the deductions of the function dw/du at these points, for example, at point E ($u = \pi\tau/2$) there is a source with intensity $4hv_0$ (the fourth part of this source is the intensity of the incoming jet hv_0). The deduction of the function dw/du at point E is related to the intensity of the source by the formula

$$2\pi i \operatorname{Res}_{\pi\tau/2}\left[\frac{dw}{du}\right] = 4 i h v_0$$

Using the expression for the deduction of the complex function dw/du with a zero-converting function in the denominator (the function ϑ_4 has zero of the first order at the point $u = \pi\tau/2$), we obtain the following expression for the deduction at the point $u = \pi\tau/2$

$$\operatorname{Res}_{\pi\tau/2}\left[\frac{dw}{du}\right] = N_1 \frac{\vartheta_2(\pi\tau/2 - ia)\vartheta_2(\pi\tau/2 + ia)\vartheta_2(\pi\tau/2)}{\vartheta_1(\pi\tau/2)\vartheta_3(\pi\tau/2)\vartheta_4'(\pi\tau/2)}$$

Using the properties of theta functions and the formula for the derivative $\vartheta_1' = \vartheta_2\vartheta_3\vartheta_4$ (here the argument of functions $u = 0$), we obtain the formula relating the constant N_1 to the jet width h:

$$-\pi N_1 \left(\frac{\vartheta_3(ia)}{\vartheta_2\vartheta_4}\right)^2 = 2hv_0 \ . \ (3)$$

Doing the same procedure for point D ($u = 0$), where there is a runoff of intensity $4\Delta v_0$, and using the law of conservation of mass, we obtain the following expressions for the thickness of the jets:

$$\frac{\Delta}{hv_0} = \left(\frac{\vartheta_2(ia)\vartheta_2}{\vartheta_3(ia)\vartheta_3}\right)^2 \ , \ \frac{\delta}{h} = 1 - \left(\frac{\vartheta_2(ia)\vartheta_2}{\vartheta_3(ia)\vartheta_3}\right)^2$$

Note that the functions ϑ_2 и ϑ_3 of the imaginary argument have real values, and at $a = \pi|\tau|/2$ (given that $\vartheta_2(\pi\tau/2) = q^{-1/4}\,\vartheta_3$ and $\vartheta_3(\pi\tau/2) = q^{-1/4}\,\vartheta_2$) the thickness of the backflow reverses to zero.

2.4 Determinations of geometric characteristics of the flow

Let's introduce the function $f(u) = \dfrac{dz}{du} = \dfrac{dz}{dw}\dfrac{dw}{du} = N_1 e^{2i\frac{\beta}{\pi}u}\dfrac{\vartheta_2^2(u+ia)\vartheta_2(u)}{\vartheta_1(u)\vartheta_3(u)\vartheta_4(u)}$.

The coordinate of the flow separation point B in the physical plane $z_B = x_B + i\,y_B$ can be found by calculating the integral

$$z_B = \int_{u=\pi/2}^{u=\pi/2+ia} f(u)du$$

Let's choose as a curve connecting the points $\pi/2$ and $\pi/2 + ia$ the line $u = \pi/2 + i\eta$. For numerical solution it is convenient to pass to the system of equations

$$\begin{aligned}\frac{dx}{d\eta} &= -\mathrm{Im}\left[f(\pi/2+i\eta)\right]\\ \frac{dy}{d\eta} &= \mathrm{Re}\left[f(\pi/2+i\eta)\right]\end{aligned}. \qquad (4)$$

The system (4) is solved with initial conditions at $\eta = 0;\ x = 0, y = 0$ на интервале $\eta \in [0, a]$.

To determine the width of the gap between the plate edge and the horizontal plane *ED* (the width of the nozzle outlet section *d*), we find the coordinate of some point A', lying on the line *E, D* (Fig. 12c). For definiteness, let the point A' be $u = \pi\tau/4$ and let the integration curve in the plane u be a straight line connecting the points *A* and : A' $\eta = |\tau|(\pi/4 - \xi/2)$. For a complex variable we can write $u = \xi + i|\tau|(\pi/4 - \xi/2)$. Considering these formulas and separating the real and imaginary parts, we obtain a system of equations

$$\begin{aligned}\frac{dx}{d\xi} &= \mathrm{Re}\left[f(u)\right] + \frac{|\tau|}{2}\mathrm{Im}\left[f(u)\right]\\ \frac{dy}{d\xi} &= \mathrm{Im}\left[f(u)\right] - \frac{|\tau|}{2}\mathrm{Re}\left[f(u)\right]\end{aligned}. \qquad (5)$$

The system (5) is integrated with initial conditions:$\xi = \pi/2;\ x = 0, y = 0$. Integration is performed on the interval $\xi \in [\pi/2, 0]$. Let us denote the end point on the sloping line (at $\xi = 0$): x_n, y_n, then we can determine the nozzle width: $d = |y_n|$. Setting the parameter a equal to the limiting value (2), we obtain the limiting nozzle width at the given $v_0(\le 1), \beta$, the jet thickness h can be set equal to 1. When increasing the parameter a, the width of the outlet nozzle will decrease and there will be a return jet of liquid with width δ.

To determine the shape of the jets, integrating along the horizontal sides of the auxiliary rectangle yields quite simple equations:

$$\begin{aligned}\frac{dx}{d\xi} &= \mathrm{Re}\left[f(\xi)\right]\\ \frac{dy}{d\xi} &= \mathrm{Im}\left[f(\xi)\right]\end{aligned}\ \text{for jet } A, D \qquad \begin{aligned}\frac{dx}{d\xi} &= \mathrm{Re}\left[f(\xi + i\,\pi|\tau|/2)\right]\\ \frac{dy}{d\xi} &= \mathrm{Im}\left[f(\xi + i\,\pi|\tau|/2)\right]\end{aligned}\ \text{for } E, C. \qquad (6)$$

For jets *A, D* at $\xi = \pi/2;\ x = 0, y = 0;$ the integration is carried out over the interval $\xi \in [\pi/2, 0]$ with the coordinates of the jet points given in some step along ξ. It is somewhat more difficult to determine the coordinates of points at the boundary *C, E* (cavern boundary) here the integration

along *CE* was carried out with accuracy to the complex constant, which was determined from satisfaction of asymptotic conditions at the remote points *E* and *C* (that is, the jet boundary should extend to jets of known thickness - *h* and δ) .

2.5 Calculation results

We will consider the case $v_0<1$. Here, the peculiarity of the solution is that for given physical parameters ($\alpha=\pi-\beta$ - angle of inclination, *d* - width of the gap between the edge of the inclined plate and the flat bottom) there is a critical value of the parameter a (follows from (2), at which the jet (cavern) touches the inclined plate at point *B,* which is at a finite distance from the plate edge (point *A*). The thickness of the return jetδ is zero. The jet surface in this case is unstable in the Rayleigh-Taylor sense (acceleration is directed from the "light phase" to the "heavy phase"). Earlier it was experimentally shown [1] that the stationary boundary of the jet in this case can be considered as an unperturbed surface relative to which the perturbations develop. The stationary solution makes it possible to determine the geometrical characteristics of such a flow region and, involving additional hypotheses (see below), knowing the acceleration at the jet boundary, to estimate the parameters of Rayleigh-Taylor structures.

Figure 13 shows the results of calculations for $\alpha=45^0$ and $d = 0.4$, critical flow conditions here are realized at $v_0= 0.3$ ($C_d=1-v_0^2 = 0.91$) - curve *1* (red). The thick lines represent the inclined plate and the horizontal bottom (or axis of symmetry) bounding the flow. The curvature of the cavern boundary under critical flow conditions is such (the acceleration at the boundary is directed from the "light" fluid to the "heavy" fluid) that the liquid-gas interface in the surging jet is unstable in the Rayleigh-Taylor sense. The curvature at the *EB* boundary (and therefore the acceleration) increases monotonically from zero (at point *E*) to infinity at the point where the cavern closes on the inclined plate *B*, which is at a finite distance from the edge of plate *A*. The jet flowing outward is also shown in red. It can be seen that a small decrease in the cavern pressure coefficient C_d by only 0.7% (curve *2*), leads to a significant decrease in the instability region and then to the disappearance of such a region (curves *3* and *4*). This indicates the narrowness of the region of existence of such modes, which is confirmed by experiment (Fig. 10). However, the same experiment shows that such modes really exist. It should be borne in mind that when $C_d$increases beyond the critical value in the framework of the accepted model, the solution does not exist, the stationary jet can no longer interact with the inclined wall; in reality, the mixing process continues and even intensifies [2]. So the mechanism of P-T mixing can be extended into the subcritical region, and this regime can depend on the length of the *shaft* section. In Fig. 13 and further, all lengths are referred to the jet width *h*.

Figure 14 shows a comparison of critical flow boundaries for different $d = 0.013, 0.2, 0.4, 0.6, 0.8$ (jet boundaries are shown in red). These values of *d* correspond to the following values of

dimensionless velocity v_0 = 0.01, 0.15, 0.3, 0.462, 0.67 or C_d = 0.9999, 0.978, 0.91, 0.787, 0.551. The pressure coefficient of the critical flow regime separates the regions of different types of autoconvulsions. It was noted earlier that low-frequency autoconvulsions occur at cavern pressure coefficients larger than the above critical values. Fig. 14 shows that as the nozzle width decreases, the critical velocity v_0 decreases (the pressure in the cavern increases) and the distance between the cavern connection point and the nozzle edge increases.

Fig. 15 shows the picture of free boundaries of the flow for 4 angles of plate inclination and for nozzle outlet section width - 0.4. For inclination angles of 30º, 45º, 45º, 90º, 135º and nozzle width of 0.4, the critical regime occurs at v_0 = 0.325, 0.3, 0.263, 0.253. It can be seen that the critical value of v_0 (and C_d) depends weakly on the plate inclination angle, but as the angle decreases (less than 90º), the distance from the point of cavern attachment to the plate edge starts to increase strongly; at angles larger than 90º, the dependence of the flow pattern on the angle almost disappears.

The dependences of the pressure coefficient and the distance from the point of cavern closure to the plate edge on the gap d for critical flow conditions shown in Fig. 16 show that the critical pressure coefficient depends weakly on the plate inclination angle and is mainly determined by the gap d. But the position of the cavern attachment point strongly depends on the plate inclination.

In the problem of jet reversal under the action of a pressure drop [1], there was a flow region with constant curvature of the cavern boundary. In the considered case, the curvature of the cavern grows monotonically from zero at the infinitely distant point E to infinity at the point where the cavern joins the plate B. For qualitative evaluation, let us introduce some effective value of the cavern curvature radius R_c, equal to the radius of the circle touching the inclined plate at point B and the horizontal line Y= 1 corresponding to the jet boundary at point E (at infinity). The acceleration of the fluid particles on the circle can be estimated as $W_c = v_0^2/R_c$. As the oscillogram (Fig. 11) shows, the high-frequency auto-oscillatory mode has a single-mode (single-frequency) character. For the case of single-mode mixing, a formula [16] for the velocity of Rayleigh-Taylor bubbles at large values of time is obtained $v_b = 0.23\sqrt{\lambda W_c}$, where the wavelength is $\lambda = v_0/f$ (we deal with standing waves relative to the liquid), and the frequency can be related to the Struhal number $f = (V_\infty/D_c)\mathrm{Sh}$. Then for the velocity of the bubble motion we can write

$$\frac{v_b}{V_\infty} = 0.23 v_0 \sqrt{\frac{v_0}{\frac{R_c}{h}\frac{h}{D_c}\mathrm{Sh}}}$$

For our conditions of jet inflow through the hole of width D_c from a wide pipe (the ratio of D_c to the width of the supply pipe is 0.22) the value of h/D_c is approximately equal to 0.62, we will take the Struhal number from the experiment (Fig. 11): Sh=0.13. Let us estimate the penetration

depth of the Rayleigh-Taylor bubbles L_b, related to the jet width h, for plate inclination angles 45 and 90^0, by the velocity $v_b$and the time of passing the corresponding arc of a circle of radius R_c with velocity v_0. So, the formula for the motion of P− T-bubbles is obtained under the following assumptions: 1) the cavern can be replaced by some effective circle, 2) the development of P− T-structures occurs in the regime of single-mode mixing, 3) the frequency characteristics of the shafts can be taken from a similar axisymmetric experiment.

Fig. 17 shows the depth dependences of the Rayleigh-Taylor structures moving inside the jet for the time of passing the arc of the effective circle (with rotation by 45 and 90^0, red and green color) - solid curves. For comparison, the curves for the depth L_{bb}, obtained under the assumption that the development of structures follows the same law when the fluid moves along the plate at the *shaft* section. It can be seen that, if we evaluate the development of structures, only on the arc of the circle the evolution of bubbles for 45 and 90^0 is approximately the same, taking into account the *shaft* section for $90^0$the difference is not noticeable, but for 45^0 (see dashed curve) is quite significant. Depending on the width of the nozzle exit cross-section, there is a maximum depth of penetration of the Rayleigh-Taylor structures into the jet, and the depth of this displacement is quite comparable to the width of the expelling jet, equal to the corresponding value of $v_{(0)}$.

CONCLUSION

The research of auto-oscillatory flow modes was carried out on an axisymmetric model of a cavitation generator of pulse jets with a central location of a jet flowing out of an orifice in a diaphragm with a diameter of 10 mm. The efficiency of the generator was determined by the intensity of the shock impact of the expiring jets on the screen - obstacle.

There is a maximum as a function of the nozzle outlet cross-section diameter - the highest impact intensity is observed at an outlet cross-section diameter of 7 mm.

It was found that the intensity of shock pulses on the screen as a function of the distance to the screen falls approximately proportional to the square root of the distance.

A narrow region of existence of high-frequency autoconvulsions with very low intensity of pressure fluctuations in the cavern and significant impulse effects on the screen-obstacle was found at relatively small gas blow-ups. This may be related to the occurrence of the Rayleigh-Taylor instability of the cavern boundary with increased pressure compared to the external pressure. This assumption is justified by the analysis of the obtained exact solution of the plane problem on the interaction of a finite jet moving along a plane wall (plane of symmetry) with an inclined plate at different pressures on the surfaces of the advancing and expiring jets.

It is shown that a stationary flow with an unstable Rayleigh-Taylor boundary is indeed realized near the limiting flow when the thickness of the return jet turns to zero and the incoming

jet touches the inclined plate at some point above the plate's disruptive edge. The relationship between the cavern pressure coefficient (or cavitation number), the plate inclination angle, and the width of the gap between the plate disruption edge and the symmetry plane is obtained. With the adoption of a series of assumptions and using experimental data, estimates of the depth P− T-stirring have been made, showing that this depth is comparable to the width of the expelling jet.

REFERENCES

1. *Kozlov I.I., Prokofiev V.V.* Laws of wave development on the surface of a cavern with a negative cavitation number // Reports of the Russian Academy of Sciences. 2006. V. 409. № 1. P. 43-47.
2. *Kozlov I.I., Ocheretyanyi S.A., Prokofiev V.V.* Auto oscillatory modes in a liquid jet curtain separating gas regions with different pressures // Izv. RAS MZhG. 2013. № 6. P. 33-43.
3. *Ocheretyanyi S.A., Prokofiev V.V.* Effect of nozzle constriction on the operation of a periodic pulse jet generator // Izv. RAS MZhG. 2022. № 2. P. 14-26.
4. *Atanov G.A., Semko A.N.* Numerical Analysis of the Jet Flows of Compressible Water // Proc. of International Summer Scientific School "High Speed Hidrodynamics". June 2004, Cheboksary. Computational Publications. Russia. 2004. P. 39-44.
5. *Semko A.N.* Impulse jets of high-speed liquid and their application: monograph // ed. by Semko A. *N*. Donetsk: *DonNU*. N. Donetsk: DonNU. 2014. 370 p.
6. *Savchenko N.V., Yakhno O.M.* Hydrodynamic methods of creating pulsating jets for hydrodestruction of solid materials // Bulletin of Sumy State University. Ser.: Technical Sciences. 2003. № 12(58). P. 92-98.
7. *Pilipenko V.V.* Cavitation auto oscillations. Kiev: Naukova Dumka. 1989. 318 p.
8. *Zhulai Yu.A., Dzoz N.A., Zadontsev V.A., Burylov S.V., Novikov V.F.* Possibility of track structure cleaning by pulsating and cavitating water jets during the rolling stock movement // Science and progress of transport. Bulletin of Dnepropetrovsk National Un-ta of Railway Transport named after Academician V.Lazaryan. 2005. № 8. P.151-155.
9. *Prokofiev V.V., Ocheretyanyi S.A., Yakovlev E.A.* Use of cavitation auto-oscillation modes for generation of periodic pulse jets (in Russian) // PMTF. 2021. V. 62. № 1. P. 97-108.
10. *Ocheretyanyi S.A., Prokofiev V.V.* Influence of cavitator and nozzle parameters on the efficiency of the pulse jet generator // Izv. RAS MZhG. 2023. № 5. P. 10-24.

11. *Kozlov I.I., Ocheretyanyi S.A., Prokofiev V.V.* About different modes of auto oscillations in the flows with a ventilated cavern and the possibility of using them for the formation of periodic pulse jets. // Izv. RAS. MZHG 2019. № 3. P. 16-27.
12. *Tolokonnikov S.L.* Liquid flow through a slit in a flat wall in the presence of a variable intensity source on the symmetry plane of the flow. // MSU Vestnik. Ser.1. Mathematics. Mechanics. 2017. № 3 P. 40-45.
13. *Kozlov I.I., Prokofiev V.V., Puchkov A.A.* Research of the wave structures development on the unstable boundary of a cavern by means of a high-speed video camera (in Russian) // Izv. RAS. MZHG 2008. № 2. P. 137-148.
14. *Gurevich M.I.* Theory of ideal liquid jets. Moscow: Nauka, 1979. 536 p.
15. *Birkhoff G., Zarantonello E.H.* Jets, Wakes and Cavities. New York. Academic Press Inc. Publishers. 1957. Translation from English. Birkhof G., Sarantonello E. Jets, traces and caverns. M.: Mir, 1964. 466 p.
16. *Herzenstein S.Ya., Kozlov I.I., Prokofiev V.V., Reznichenko N.T.,* Chernyi *G.G., Chernyavskii V.M.* Rayleigh-Taylor instability in the Hele-Shaw cell: influence of initial perturbations (in Russian) // Izv. RAS. MZHG 2008. № 3. P. 12-18.

FIGURE CAPTIONS

Fig. 1. Scheme of the axisymmetric experiment setup.

Fig. 2. Dependence of C_d on C_q for P_0=0.15 MPa, nozzle cylindrical length 11 mm, distance to the target disk 25 mm, for 4 diameters of the outlet section (5, 6, 7, 8 mm).

Fig. 3. Dependence of Sh *on* C_q for P_0=0.15 MPa, nozzle cylindrical length 11 mm, distance to the target disk 25 mm, for 4 diameters of the outlet section (5, 6, 7, 8 mm).

Fig. 4. Dependence of A_k/P_0 on C_q for P_0=0.15 MPa, nozzle cylindrical length 11 mm, distance to the target disk 25 mm, for 4 diameters of the outlet section (5, 6, 7, 8 mm).

Fig. 5. Dependence of A_m/P_0 on C_q for P_0=0.15 MPa, nozzle cylindrical length 11 mm, distance to the target disk 25 mm, for 4 diameters of the outlet section (5, 6, 7, 8 mm).

Fig. 6. Dependence of the pressure coefficient $C_d$on the gas flow coefficient C_q at P_0=0.15 MPa and different distances to the target disk.

Fig. 7. Dependence of Struhal number on the gas flow coefficient at P_0=0.15 MPa and different distances to the target disk.

Fig. 8. Dependence of the relative intensity of pressure pulsations in the cavern on the gas flow coefficient at P_0=0.15 MPa and different distances to the target disk

Fig. 9. Dependence of the relative intensity of impact on the target disk on the gas flow coefficient at P_0=0.15 MPa and different distances to the target.

Fig. 10. Dependence of Sh (a), and relative intensities on the screen (b) on the gas blow-up ratio for a nozzle with a cylindrical length of 36 mm and an outlet cross-section of 6 mm at head pressure P_0= 0.15 MPa (solid lines) and 0.2 MPa (dashed lines).

Fig. 11. Oscillogram of the high-frequency mode at P_0=1.54 atom, C_q=4.5, *D=10* mm, with nozzle length of 36 mm, with an outlet section of 6 mm diameter (a); mplitude-frequency spectra of pressure pulsations on the screen (b) and in the cavern (c). The amplitudes are normalized by the maximum value.

Fig. 12. Flow in the physical plane $z\ x=+$ iy (a), plane of complex. Potential $w = \phi + i\,\psi$ (b), auxiliary plane $u = \xi + i\,\eta$ (c).

Fig. 13. Free boundary picture atα =45º and *d*= 0.4, t. A is the plate edge, B is the point where the cavern joins the plate. *1* critical flow, v_0=0.3 (C_d=0.91), *2* – v_0=0.31 (C_d=0.904), *3* – v_0=0.33 (C_d=0.891), *4* – v_0=0.4 (C_d=0.84).

Fig. 14. Free boundary picture for plate tilt angle 45º and *d=0*.013, 0.2, 0.4, 0.6, 0.8.

Fig. 15. Free boundary picture at the critical flow regime for *d=0*.4 and plate inclination angles of 30º, 45º, 90º, 135º (*1-4*, respectively).

Fig. 16. Dependences of the critical pressure coefficient (C_d) and the distance from the cavern closure point *B(L)* to the plate edge on the gap width *d/h* under the critical flow regime for inclination angles of 45º and 90º.

Fig. 17. Dependence of the penetration depth of Rayleigh-Taylor structures $L_b/\ L_{bb}$ on the exit section width d/h for plate inclination angles of 45 and 90º.

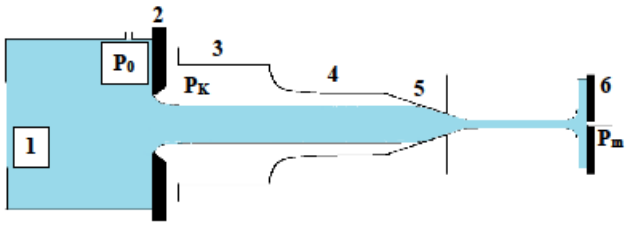

Fig. 1.

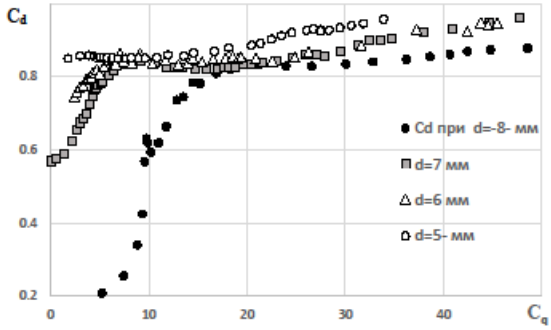

Fig. 2.

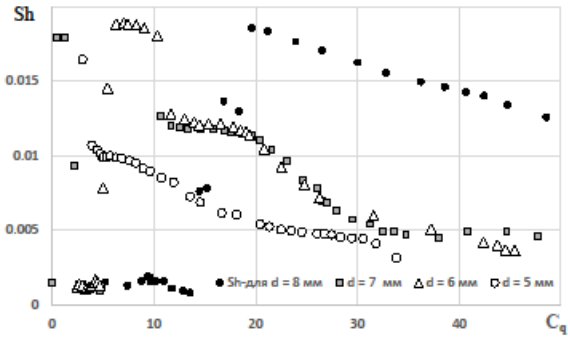

Fig. 3.

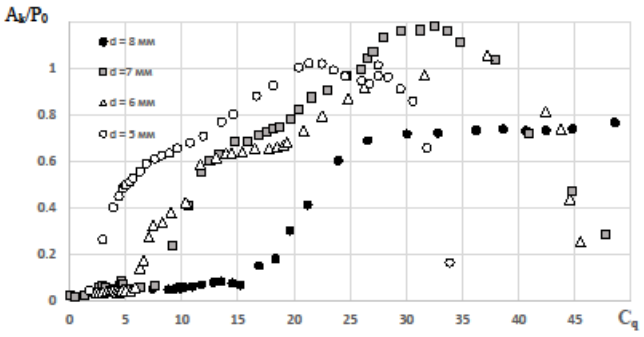
$A_ж/P_0$
d = 8 мм
d = 7 мм
d = 6 мм
d = 5 мм
0
0.2
0.4
0.6
0.8
1
0
5
10
15
20
25
30
35
40
45
C_q

Fig. 4.

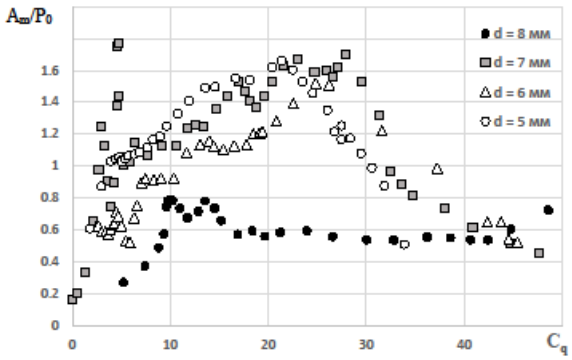

Fig. 5.

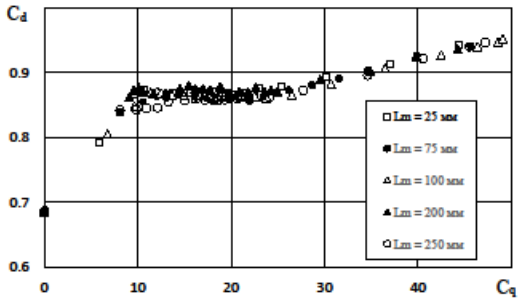
Cd
0.9
0.8
0.7
0.6
0
10
20
30
40
Cq
Lm = 25 мм
Lm = 75 мм
Lm = 100 мм
Lm = 200 мм
Lm = 250 мм

Fig. 6

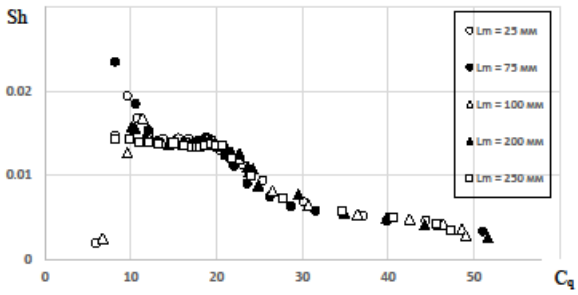
Sh
0.02
0.01
0
0
10
20
30
40
50
C_q
Lm = 25 мм
Lm = 75 мм
Lm = 100 мм
Lm = 200 мм
Lm = 250 мм

Fig. 7.

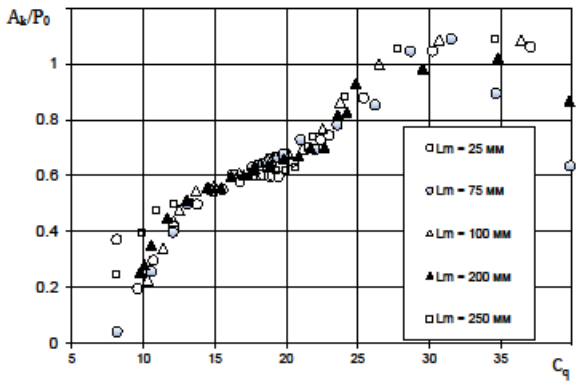
A_k/P_0
1
0.8
0.6
0.4
0.2
0
5
10
15
20
25
30
35
C_q
Lm = 25 мм
Lm = 75 мм
Lm = 100 мм
Lm = 200 мм
Lm = 250 мм

Fig. 8.

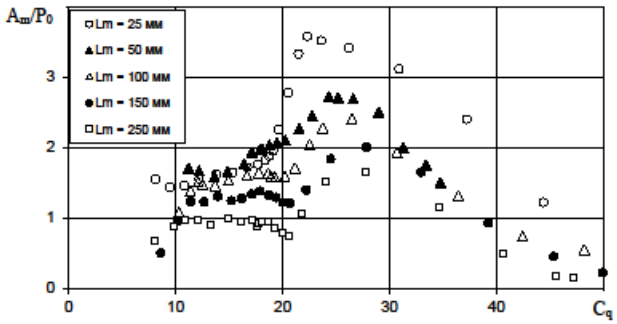
Am/P0
Lm = 25 мм
Lm = 50 мм
Lm = 100 мм
Lm = 150 мм
Lm = 250 мм
0
1
2
3
0
10
20
30
40
Cq

Fig. 9.

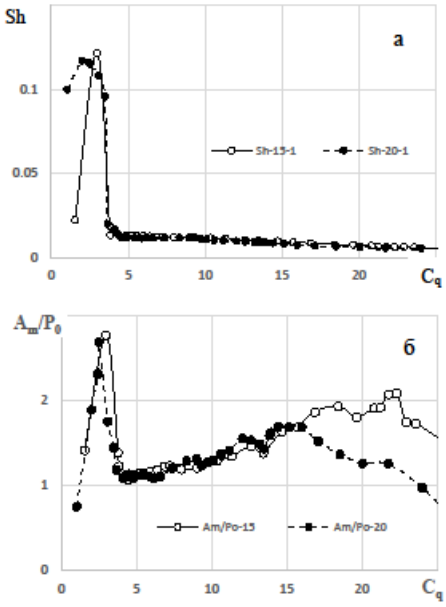
Sh
а
0.1
0.05
0
Sh-15-1
Sh-20-1
0
5
10
15
20
Cq
Am/P0
б
2
1
0
Am/Po-15
Am/Po-20
0
5
10
15
20
Cq

Fig. 10.

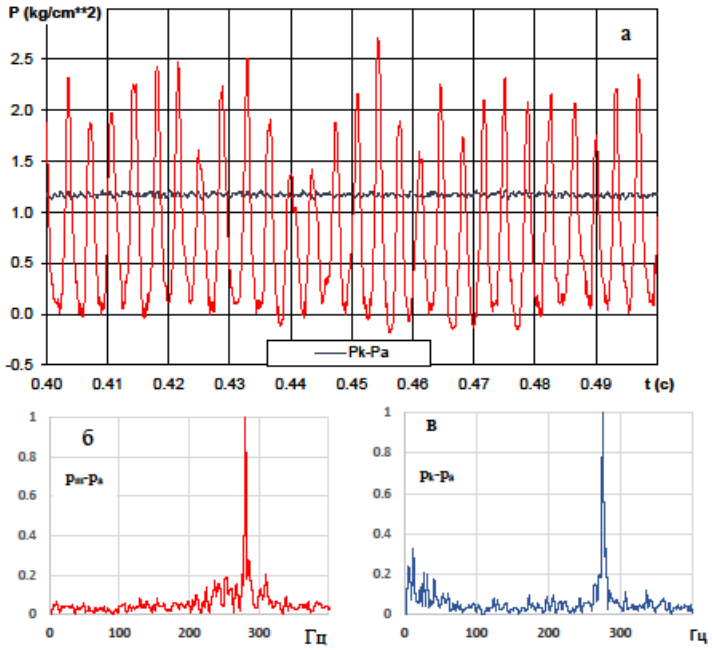
P (kg/cm**2)
a
2.5
2.0
1.5
1.0
0.5
0.0
-0.5
Pk-Pa
0.40 0.41 0.42 0.43 0.44 0.45 0.46 0.47 0.48 0.49 t (c)
б
1
0.8
0.6
0.4
0.2
0
0 100 200 300 Гц
в
1
0.8
0.6
0.4
0.2
0
0 100 200 300 Гц

Fig. 11.

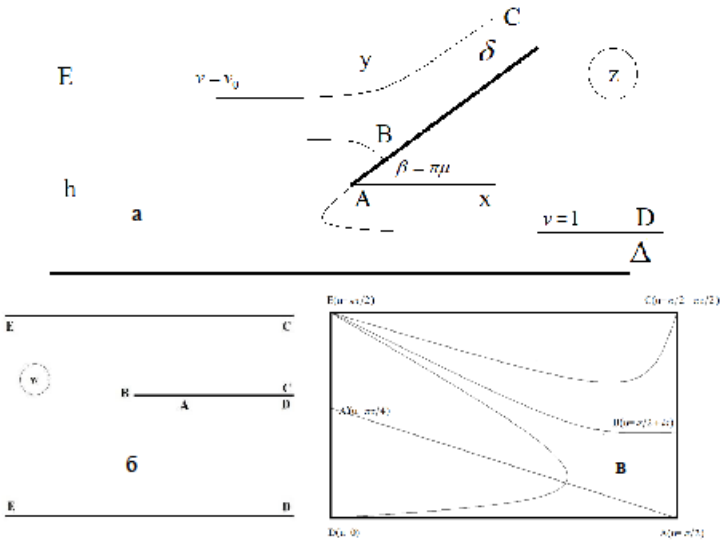

Fig. 12.

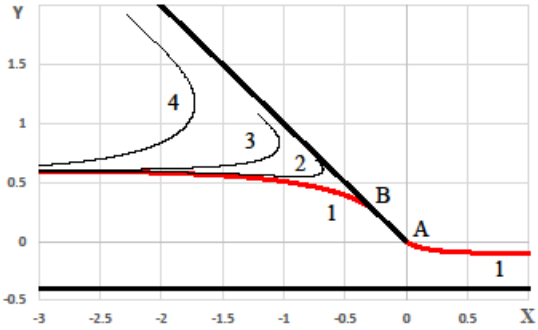

Fig. 13.

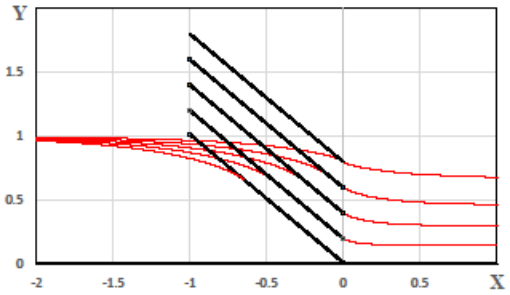

Fig. 14.

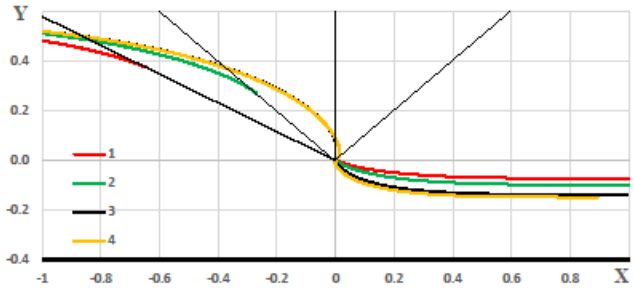

Fig. 15.

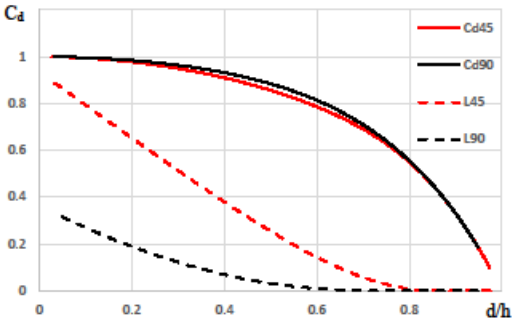

Fig. 16.

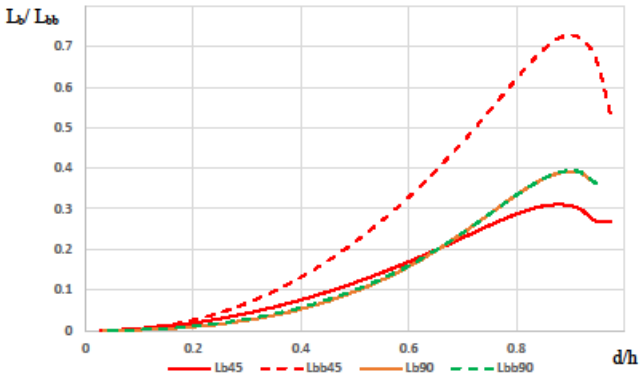

Fig. 17.